Available online at www.sciencedirect.com
SCIENCE DIRECT
Journal of the European Ceramic Society 26 (2006) 2441–2452
www.elsevier.com/locate/jeurceramsoc

Understanding the fretting wear of Ti_3SiC_2

Debasish Sarkar, B.V. Manoj Kumar, Bikramjit Basu *

Laboratory for Advanced Ceramics, Department of Materials and Metallurgical Engineering, Indian Institute of Technology, Kanpur 208016, India

Received 1 December 2004; received in revised form 5 May 2005; accepted 19 May 2005
Available online 28 July 2005

Abstract

The objective of the present research is to understand the tribological properties of Ti_3SiC_2. The fretting wear experiments were conducted on hot pressed Ti_3SiC_2 against bearing steel under varying load (1–10 N). Under selected fretting conditions, Ti_3SiC_2/steel couple exhibits higher COF of 0.5–0.6. Based on the detailed AFM analysis of the worn surface, the roughness parameters and bearing area of the worn surfaces are also evaluated. SEM–EDS analysis indicates the mutual material transfer between the counterfaces at the fretted contacts. Raman spectroscopy reveals that the fretting wear is accompanied by triboxidation with the formation of TiO_2, SiO_2 and Fe_2O_3. An important observation is that 'metal-like plasticity' behavior is observed on worn Ti_3SiC_2 at higher load (>6 N). A probable explanation for the transition in friction and wear with load is proposed.

Keyword: Friction; Wear resistance; Electron microscopy; Spectroscopy; Plasticity; Ti_3SiC_2

1. Introduction

Since the discovery of a vast number of ternary carbides and nitrides by Jeitschko and Nowotny,[1] Ti_3SiC_2 has received attention in the materials community.[2–12] Recently, Barsoum[2] identified that these phases represent a new class of solids that can be described as thermodynamically stable laminates. These exhibit both metallic and ceramic features.[2] This class of materials was lately named as MAX phases, because of their chemistry: ternary layered hexagonal carbides and nitrides, with the general formula $M_{n+1}AX_n$, where $n = 1–3$, M is an early transition metal, A belonging to III–VIA group of periodic table and X is either C and/or N. The physical properties (thermal and electrical conductivity) and mechanical behavior of ternary carbides, in particular Ti_3SiC_2 have been investigated with a focus to understand the structure–property correlation.

Some of the key properties of Ti_3SiC_2 include excellent resistance to oxidation up to 1400 °C, high thermal shock resistance, high Young's modulus (325 GPa), relatively low hardness (4–5 GPa), high fracture toughness (7–9 MPa $m^{1/2}$) and good machinability with conventional tools.[6,7] Like graphite, Ti_3SiC_2 has a hexagonal structure with a space group of *P*63/*mmc*. The crystal structure of Ti_3SiC_2, as shown in Fig. 1, can be described as a planar stacking sequence along the *c*-axis, consisting of double layers of Ti–C edge-sharing octahedra, sandwiched between sheets of square-planar coordinated Si atoms.[1] The electrical ($(2–15) \times 10^6\ \Omega^{-1}\ m^{-1}$) and thermal (20–50 W/m K) conductivities of these ternary carbides exceed those of Ti metal. The high electrical conductivity is attributed to the metallic bonding parallel to the basal plane.[5] Being readily machinable, Ti_3SiC_2 is elastically quite stiff (~320 GPa), i.e. three times stiffer than Ti metal, however, with the same density as Ti, i.e. ~4.5 gm/cc.[8] Ti_3SiC_2 is also a damage-tolerant material and has a brittle-to-ductile transition at 1200 °C. At 1300 °C, the material exhibits "yield" points at 100 and 500 MPa in flexure and compression loading, respectively.[9] The large-grained, oriented, polycrystalline form of Ti_3SiC_2, loaded in compression at room temperature, was reported to deform plastically by a combination of shear and kink-band formation.[3,4]

* Corresponding author. Tel.: +91 512 2597771; fax: +91 512 2597505.
E-mail address: bikram@iitk.ac.in (B. Basu).

0955-2219/$ – see front matter © 2005 Elsevier Ltd. All rights reserved.
doi:10.1016/j.jeurceramsoc.2005.05.006

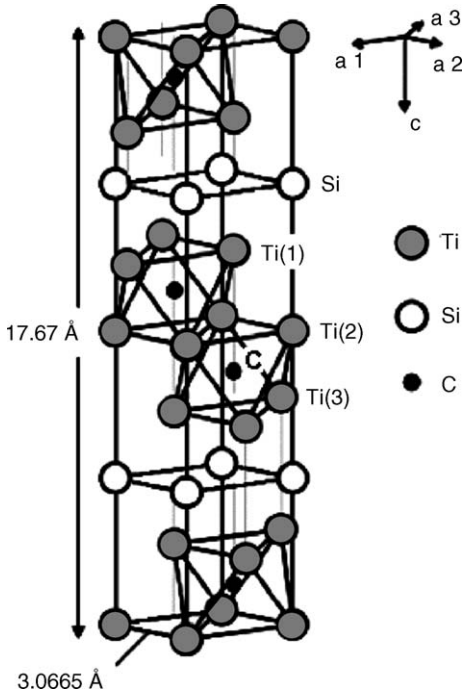

Fig. 1. Unit cell of Ti_3SiC_2.[1]

From the perspective of engineering applications, the frictional and the sliding wear resistance of Ti_3SiC_2 was evaluated to a limited extent. Myhra et al.,[10] using lateral force microscopy, measured a low kinetic friction coefficient (μ) of 0.002–0.005 at 1000–20000 nN normal force for the basal planes of Ti_3SiC_2. They also reported that μ for a polycrystalline Ti_3SiC_2, against a lightly peened stainless steel sheet, under a load of 0.15–0.9 N is ~0.12. Barsoum and co-workers reported a high coefficient of friction (COF) of 0.8 for a Ti_3SiC_2/steel tribocouple at 5 N load.[11] In their study, the frictional characteristics, as measured using pin-on-disc, were found to be independent of the microstructure of Ti_3SiC_2 (grain size varied between 5 and 100 μm). Zhang et al.[12] investigated the friction and wear behavior of self-mated Ti_3SiC_2 tribocouple and Ti_3SiC_2/diamond pairs using pin-on-flat tribometer. The friction coefficient of the former is 1.16–1.43, but that of the latter is below 0.1 for varying loads of 0.49–9.8 N load. The low friction coefficient of Ti_3SiC_2 against diamond was attributed to the formation of a lubricating film on the Ti_3SiC_2 tribosurface. In a recent report, Tang et al.[13] reported that laser melted ternary metal silicide, $Cr_{13}Ni_5Si_2$ alloy could exhibit excellent wear resistance compared to hardened 0.45% C steel and 1.0% C–1.5% Cr containing tool steel under sliding wear conditions at 98–196 N load, measured on a ball-on-wheel tribometer.

Although the above research findings briefly report the frictional properties of Ti_3SiC_2, no detailed work, according to the best of the author's knowledge, has been carried out to comprehensively understand the wear mechanism of Ti_3SiC_2. Against the above backdrop, it will be interesting to investigate the friction and wear behavior and to identify the dominant wear mechanisms involved during small amplitude of vibration (fretting) with varying load. This was the major motivation for the present work.

2. Experimental

2.1. Materials

The flat materials for tribological testing were Ti_3SiC_2, which were obtained as hot pressed discs. The green compacts containing appropriate stoichiometric amounts of commercial $TiC_{0.67}$ and Si (−325 mesh, 99.99%) are hot pressed in graphite die at 1420 °C for 90 min under Ar atmosphere at 25 MPa pressure to obtain the final density of 98–99% ρ_{th}. The larger disk specimens were machined to disks of 15 mm in diameter and 3 mm in thickness. The test surface of the disks was smoothly polished down to ~0.15 μm surface finish by wet abrasive polishing with finishing polish by diamond paste. Based on the Archimedes principle, the density of the sintered specimens was measured using water. Universal hardness tester was used to evaluate the Vickers hardness (Hv_{10}) of the composite with 10 kg load. The reported value is the average of data obtained from five indentation tests. The fracture toughness (K_{IC}) was determined by single-edged precracked beam (SEPB) method using the V-notch approach. The polished samples were etched using a 1:1:1 by volume $HF:HNO_3:H_2O$ solution and observed under scanning electron microscopy.

The Ti_3SiC_2 microstructure is characterized by platelike elongated grain (~50–200 μm) with an aspect ratio of ~8 (see Fig. 2). The unreacted fraction of TiC (bright contrast) is dispersed throughout the matrix. Based on the point-count method, the volume fraction of TiC in the investigated

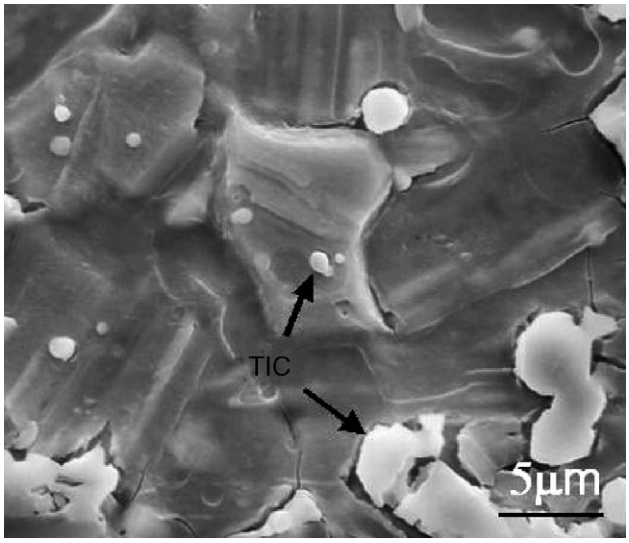

Fig. 2. SEM image of Ti_3SiC_2, etched in a 1:1:1 by volume $HF:HNO_3:H_2O$ solution. Note the presence of large elongated Ti_3SiC_2 grains and the small amount of TiC (bright contrast).

Table 1
The density and mechanical properties of the tribocouple used in our experiment

Specimen	Material	Density, ρ (gm/cc)	Hardness (GPa)	E (GPa)	Fracture toughness, K_{IC} (MPa m$^{1/2}$)
Flat	Ti_3SiC_2 (T1)	4.5	4.7 ± 0.3	316	8.9 ± 0.1
Ball (counterbody)	Steel (SAE 52100 Grade)	7.8	~7.0	210	–

Ti_3SiC_2 is measured to be 13.6. X-ray diffraction analysis also confirmed the predominant presence of Ti_3SiC_2 with a small amount of TiC. The density of the Ti_3SiC_2 flat sample was found to be 4.5 gm/cc, while that of steel ball was 7.8 gm/cc (see Table 1). The investigated polycrystalline Ti_3SiC_2 has a combination of moderate hardness (~5 GPa), lower than hardened steel (~7 GPa), and good fracture toughness (~9 MPa m$^{1/2}$), better than many structural ceramics (2–5 MPa m$^{1/2}$).

2.2. Wear tests and characterization of the surface

Based on our conceptual design and requirements, a ball-on-disk type fretting tribometer has recently been fabricated and installed in our laboratory (see Fig. 3a). Fretting is defined as small amplitude linear relative tangential sliding at constant normal load.[14,15] The computerized fretting tester has two transducers: an inductive displacement transducer sensing the movement of the flat sample and a piezoelectric transducer attached to the loading arm, monitors friction force. The friction coefficient is obtained from the on-line measured tangential force. Ti_3SiC_2 was used as a flat sample, which oscillates over the desired displacement. The commercial bearing SAE 52100 grade steel balls (hardness 63–65 HRc, data from supplier) of 8 mm in diameter were used as counterbody (stationary). This detail of the fretting set up can be found elsewhere.[16] The mechanical properties of the unworn materials are presented in Table 1. Before each test, the specimen and ball were ultrasonically cleaned with acetone. The fretting wear experiments were carried out with varying loads (1–10 N) with constant testing duration, at constant frequency (8 Hz) and constant displacement stroke (100 μm). All tests were done in air at room temperature ($28 \pm 2\,^{\circ}C$) with relative humidity (RH) $50 \pm 5\%$. The schematic of the fretting contact is shown in Fig. 3b. The combination of mode I fretting parameters results in gross slip sliding between mating surfaces across the whole contact area under the selected experimental conditions.

After each test, the worn surfaces of both the flat and the ball were ultrasonically cleaned with acetone. The wear scar profiles on each Ti_3SiC_2 sample were obtained using a computer-controlled laser surface profilometer (Mahr-Perthometer PGK 120). IR light (780 nm) is focused onto the wear scar and the reflected light from the surface is directed to a detector. With the help of a transducer, the moving position of the light is converted to an electrical signal, which is further processed to generate the 3D profile of the worn surface. The wear volume is calculated by integrating the surface area of each 2D profile (extracted from different locations on 3D profile) over distance. From the estimated wear volume, the specific wear rates [wear volume/(load × total fretted distance)] are calculated. Further detailed characterization of the worn surfaces was performed using a scanning electron microscope (FEI QUANTA 2000 HV SEM) equipped with energy dispersive X-ray analysis (EDX). The Raman spectrometer (Spectra Physics, 1877E Triplemate, USA), equipped with a nitrogen cooled charge coupled device (CCD) and argon ion laser with a wavelength of 514.52 nm, was used to study the chemistry of the tribolayer. Raman spectra were recorded in the extended scan mode with acquisition time of 300 s.

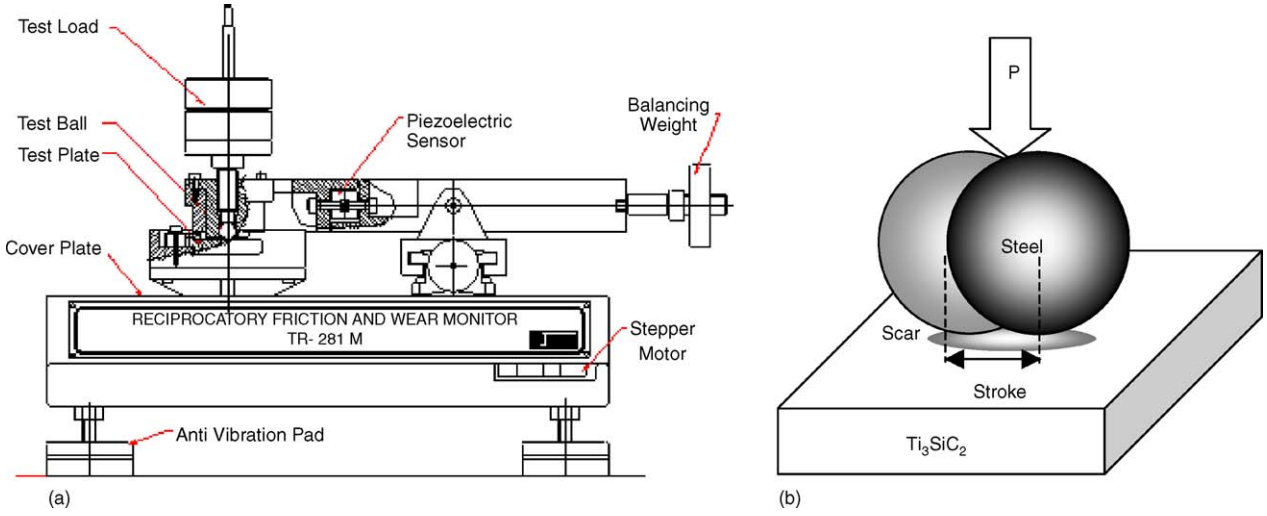

Fig. 3. A newly designed fretting set-up (a) used in the present investigation. Schematic of the fretting contact (b). The testing conditions: constants—Stroke length, 100 μm; oscillation frequency, 8 Hz and cycles 100,000. Variables—normal load (P: 2–10 N).

The major structural phases were identified using the literature reports.[17–18] The worn surface was also studied with an atomic force microscope (AFM, Molecular Imaging, Pico-SPM I, USA) using 'contact mode'. A Si_3N_4 cantilever with a three-sided pyramidal single crystal Si_3N_4 tip with apex angle of 20°, a tip radius of curvature of 10 nm and a normal stiffness of ~0.6 N/m were employed. To obtain the surface topography, typically an area of 1 μm × 1 μm of the worn surfaces after testing at 6 and 8 N were scanned with a frequency of 55 Hz and a speed of 2.2 μm/s. This technique is particularly useful to determine the surface topography and the roughness parameters of the worn surfaces.

3. Results

3.1. Friction behavior

Fig. 4 shows the plot for the frictional behavior of Ti_3SiC_2 fretted against steel with varying load. From Fig. 4, it is clear that the evolution of frictional behavior is strongly dependent on normal load as well as fretting cycles. During the running-in-period, the initial surface asperities of flat and ball get continuously knocked off and coefficient of friction (COF) increases to a high value during the first 6000, 1500 and 1000 cycles under 1, 6 and 8 N load, respectively. Then, the coefficient of friction decreased to a steady state COF of ~0.55 and 0.62 at load 1 and 6 N, respectively. At high load (8 N), the steady state COF is observed to be as ~0.5. It can be noted here that the COF of Ti_3SiC_2/steel, as measured by pin-on-disk tribometer, lies around 0.83 at 5 N load.[11] The lower COF, as measured in the present case, is presumably due to difference in contact configuration (pin-on-disk sliding versus ball-on-flat fretting) and operating parameters (sliding velocity). The frictional behavior of the investigated tribocouple will be discussed in more details in Section 4.

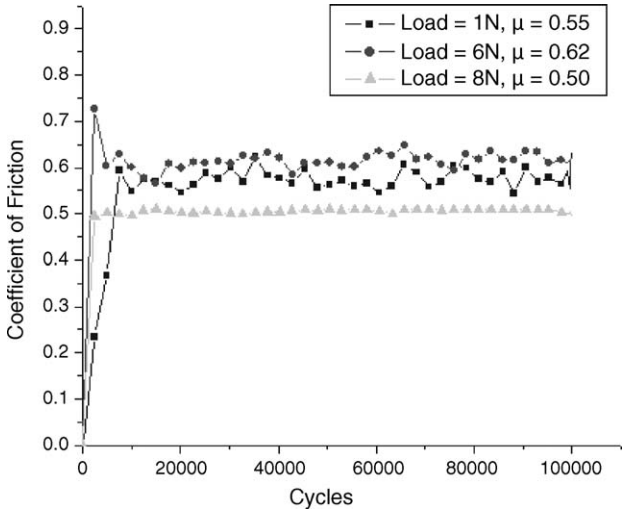

Fig. 4. Friction characteristics under different load for Ti_3SiC_2/steel fretting couple.

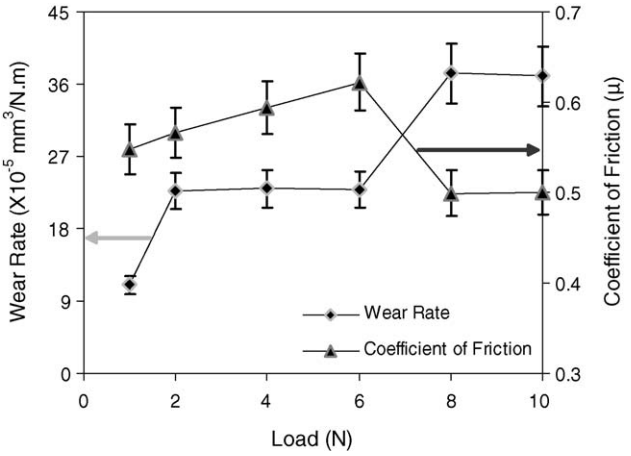

Fig. 5. The measured wear rate and coefficient of friction (μ), obtained when Ti_3SiC_2 is fretted against steel under varying loads for 100,000 cycles.

3.2. Wear behavior

3.2.1. Wear data

The wear volume, measured using laser surface profilometer, is normalized with respect to normal load and total sliding distance (number of cycles × displacement stroke × 2) to obtain the specific wear rate of Ti_3SiC_2, which is plotted against load in Fig. 5. Observing the data in Fig. 5, it is clear that wear rate varies over the same order of magnitude, i.e. 10^{-5} mm^3/N m. At the lowest load regime (1 N), the specific wear rate is low and around 10×10^{-5} mm^3/N m. The wear rate is observed to increase with load from 1 to 2 N, but does not vary much ($(20–25) \times 10^{-5}$ mm^3/N m) for fretting load of 2–6 N. However, a significant increase in wear rate is observed at 8 and 10 N load with a maximum of $\sim 37 \times 10^{-5}$ mm^3/N m recorded at 8 N load. It is interesting to note that the wear rate of hard ceramics like Al_2O_3, SiC and Si_3N_4 is measured in the order of 10^{-6} mm^3/N m (lowest up to 10^{-9} mm^3/N m).[19–21] The higher wear rate of Ti_3SiC_2 is presumably due to lower hardness (~4–5 GPa). Furthermore, it can be noted that even much higher wear rate of 10^{-3} mm^3/N m is recorded for Ti_3SiC_2 against steel using pin-on-disk tribometer.[11]

3.2.2. SEM observations

SEM images revealing the overall topography of the worn surfaces, both on flat and ball are presented in Fig. 6. Looking at the fretted area on flats, it is evident that the severity of fretting induced material damage increases with increasing load, with maximum wear at 8 N load. This is also revealed if one compares the transverse wear scar diameter, an indicative parameter to characterize the intensity of wear damage. The transverse wear scar diameter, as measured from SEM images, is ~200 μm at 1 N load and increases to ~330 μm at

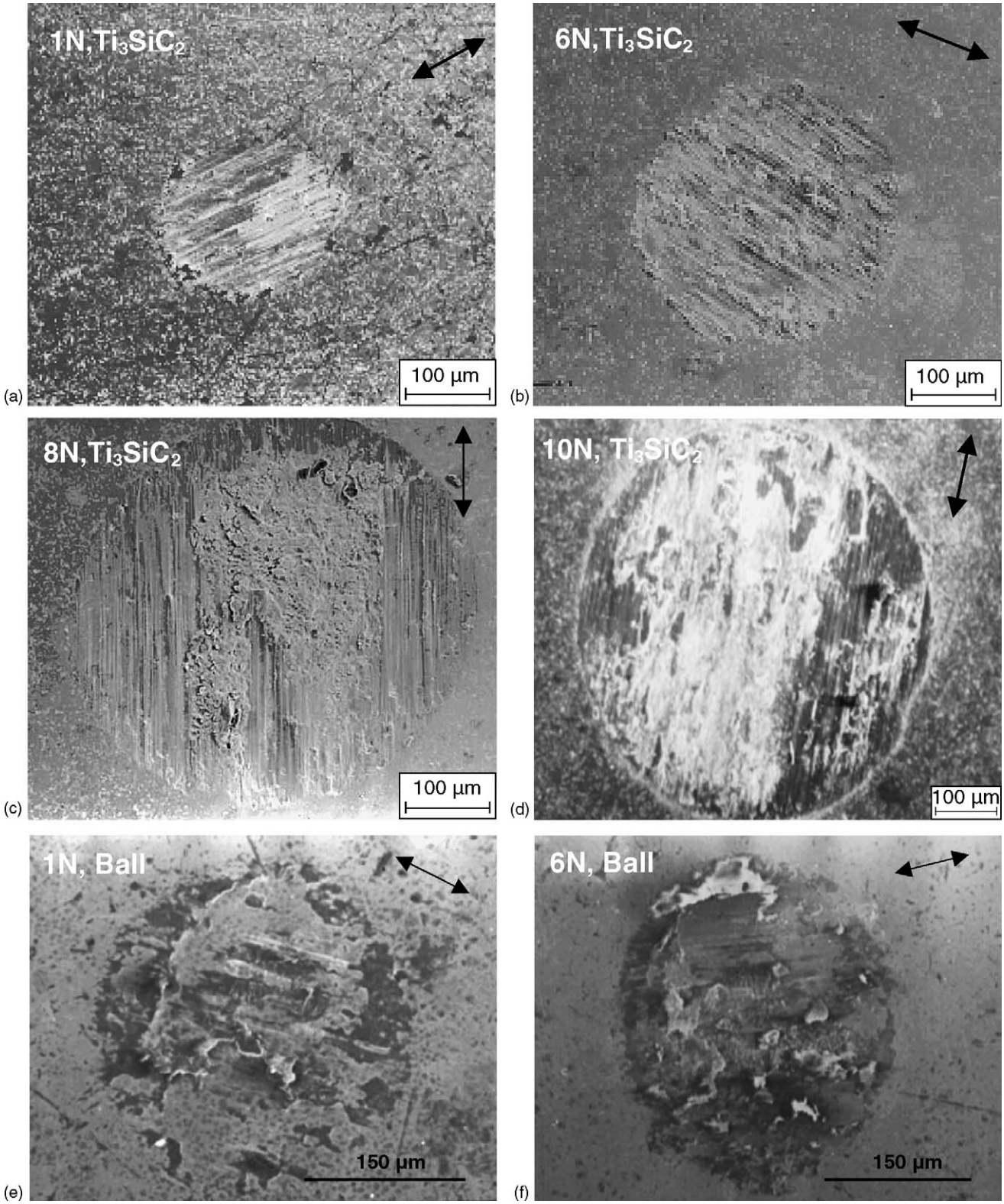

Fig. 6. SEM images revealing the overall topography of fretted zone on Ti_3SiC_2 flat (a–d) as well as steel counterbody (e and f), after fretting tests for 100,000 cycles at varying loads, as mentioned in individual figure. The pointed arrow indicates the sliding direction.

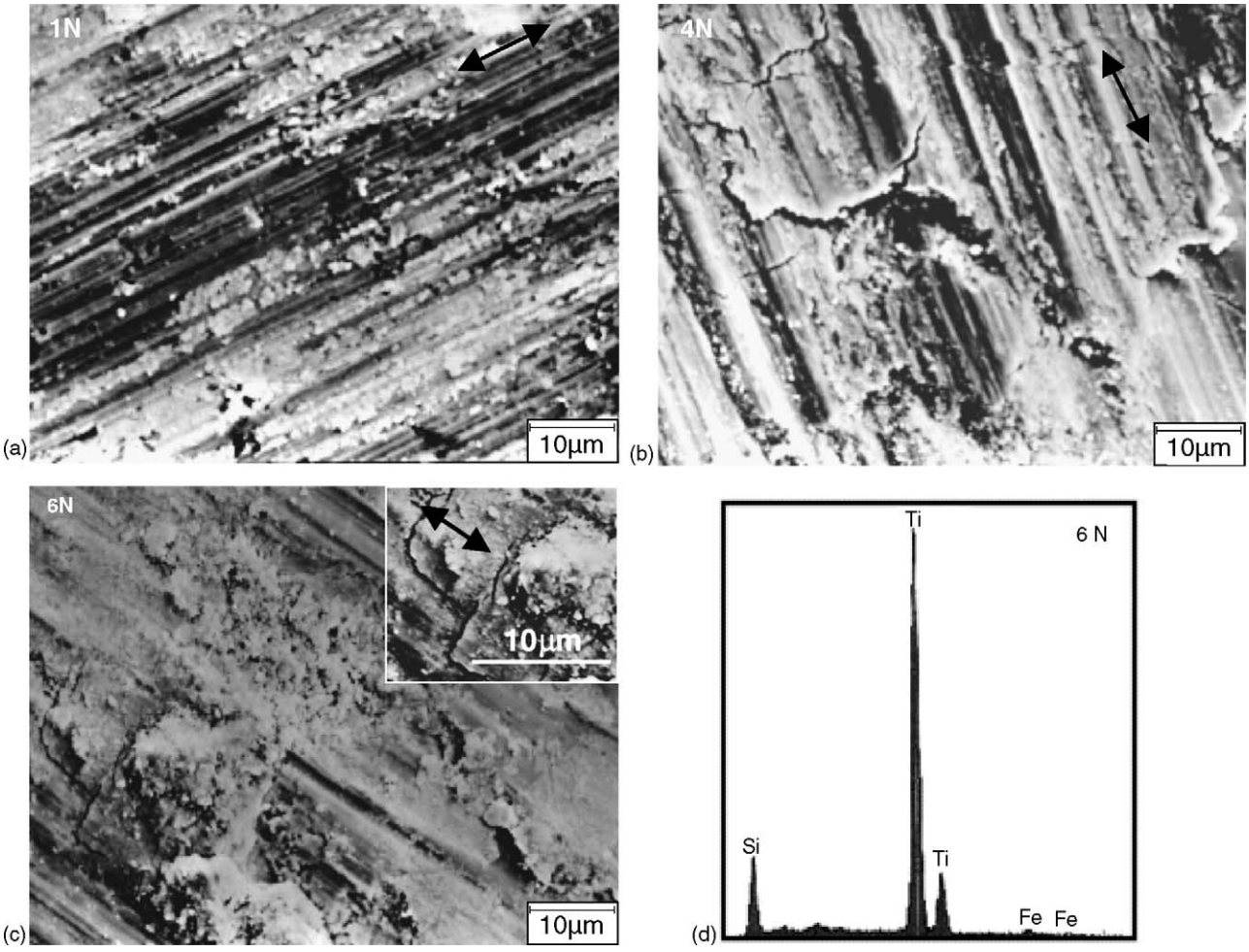

Fig. 7. SEM images showing deeper abrasive scratches of groove width around 2–3 μm (a), spalling of non-protective tribochemical layer due to propagation of cracks (b and c) on Ti_3SiC_2 worn surface after fretting against bearing steel for 100,000 cycles under varying loads, as mentioned against individual micrograph. EDS analysis indicating a small amount of Fe transfer from steel ball (d). The difference in contrast of debris particle or transfer layer with the worn base material indicates the difference in chemistry. The pointed arrow indicates the sliding direction.

6 N load. At higher loads of 8 and 10 N, the transverse wear scar diameter is maximum and around 500–510 μm.

Before we discuss the mechanisms of material removal from tribosurfaces, it is imperative to define abrasion and tribochemical wear. When the surface asperities (irregular perturbances of surface profile) from harder mating solid slide on a softer surface, the deformation or ploughing induced damage experienced by softer material is known as abrasion. When the contact is established between two mating solids, it is known as two-body abrasion. Alternatively, if the wear debris particles, generated during initial sliding, abrade the softer of the mating solids, then it is known as three-body abrasion. Tribochemical wear is usually defined as material removal process due to the chemical reactions either between a sliding body with the surrounding environment or between two moving solids, which lead to the formation of a distinct tribolayer. The chemical reactions are triggered at tribological contacts due to frictional energy. The friction and wear, in the presence of tribochemical layer largely depends on the stability or properties of the layer itself.

In the present investigation, macroscopically, it is observed that abrasion largely contributes to wear of Ti_3SiC_2 surfaces at lower loads (≤6 N). At higher loads (≥8 N), the formation of tribochemical layer and severe spalling of tribolayer is critically observed (Fig. 6c and d). While observing the fretted zone on steel counterbody, it is noted that the transverse wear scar diameter is around 150 μm at 1 N load and remains same at 6 N load (Fig. 6e and f). Also at the lowest load, the damage of steel ball appears to be more at the central region of the fretting scar, while other areas of scar do not exhibit any noticeable damage. At 6 N load, the tribochemical layer adheres on steel ball on a larger area of wear scar, compared to that at 1 N load. From the above observation, it is evident that the wear of steel ball is less compared to Ti_3SiC_2 flat, which can be expected from the hardness values (see Table 1).

Detailed topographical features of the worn surfaces after fretting at low load regime (1–6 N) are presented in Fig. 7. It is important to note that the deeper abrasive scratches of groove width around 2–3 μm are observed even at the lowest

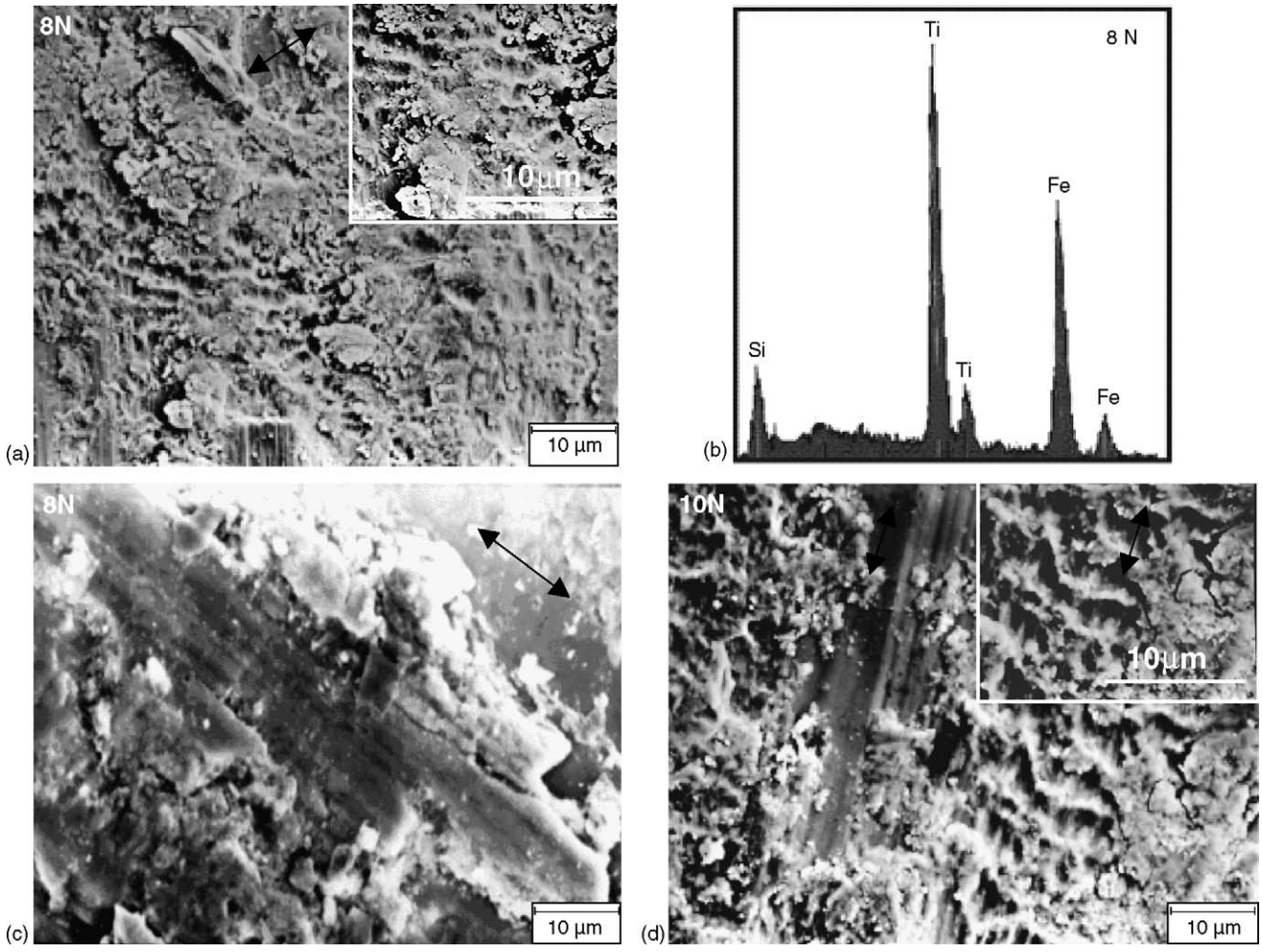

Fig. 8. SEM images showing extensive plastic deformation (a and d), EDS analysis revealing significant transfer of steel debris (b), cracks propagating along the edges of elongated grains (c) on the fretted surface of Ti_3SiC_2 after fretting against steel, for 100,000 cycles at high loads of 8 and 10 N, indicated in individual SEM image. The details of the deformed tribolayer are also shown in the inset of (a and d). The pointed arrow indicates the sliding direction.

load of 1 N. The presence of transfer layer and wear debris particles (brighter contrast) are found to adhere on the abrasive scratches (Fig. 7a). The formation of tribochemical layer is significant at 4 N load, as revealed in Fig. 7b. However, the tribochemical layer is non-protective and spalls off due to propagation of cracks, primarily in the direction perpendicular to the fretting motion. Observing the difference in electron contrast between base worn material and the tribochemical layer, it is clear that the chemistry of the later is much different from the former. Also, at 6 N load, plastically deformed layer can be observed which also contributes to the material removal (Fig. 7c). EDS analysis (Fig. 7d) reveals a smaller amount of transferred Fe from steel ball.

A clear change in worn surface topography is noted at higher loads of 8 and 10 N (see Fig. 8). The evidence of extensive plastic deformation is clear at 8 N load (Fig. 8a) and the topographical features are more like that of worn surface, commonly observed with metallic materials. The fracture of elongated Ti_3SiC_2 grains on the fretted surface is also observed and the cracks are found to propagate along the edges of elongated grains. A closer observation of Fig. 8c reveals that the fracture process aids in generation of coarser debris particles with size in the range of 5–30 μm. EDS analysis (Fig. 8b) reveals an increased transfer of steel debris at 8 N load and the transfer of steel debris particle appeared in bright contrast, as seen in Fig. 8c. At the highest load of 10 N, the contribution of plastic deformation is equally significant and the presence of cracks is also observed (Fig. 8d).

Extensive wear of steel ball is also observed, as shown in Fig. 9. At 1 N load, the severity of abrasion as well as the transfer layer with difference in compositional contrast is noted in back scattered electron (BSE) image, as shown in Fig. 9a. At the highest load of 10 N, the wear of steel ball is dominated by abrasion as well as formation of transfer layer (Fig. 9b). The compositional analysis of the worn surface using EDS reveals some interesting information. Mutual

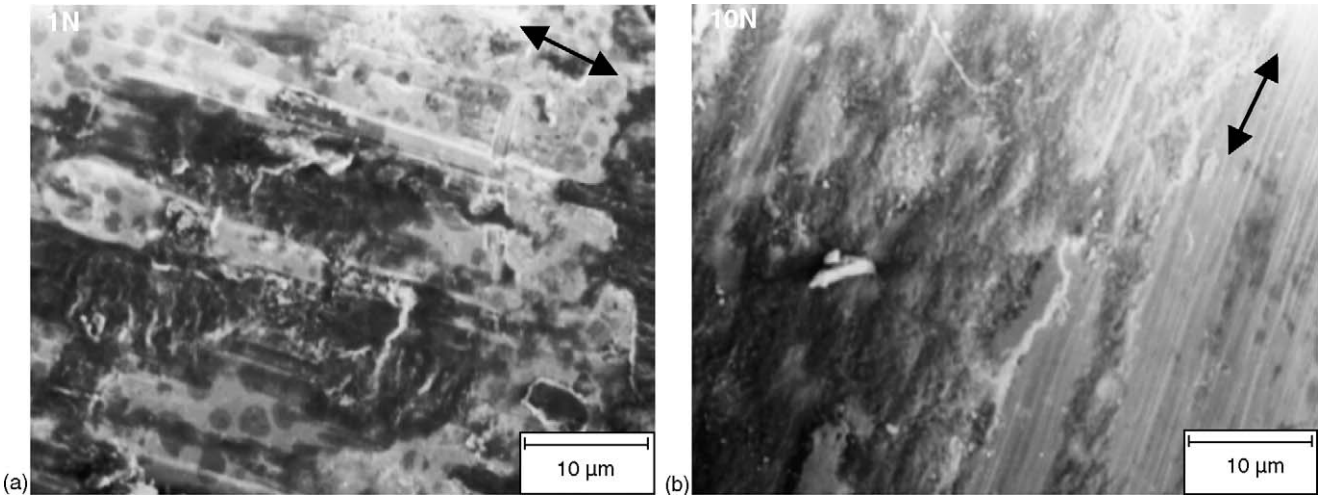

Fig. 9. SEM images of steel ball showing the abrasion, as well as the transfer layer with difference in compositional contrast at 1 N load (a) and the tribochemical layer spreading the fretted zone at 10 N load (b). The pointed arrow indicates the sliding direction.

transfer of material between Ti_3SiC_2 and steel took place during the fretting process. On Ti_3SiC_2 flat, the amount of transferred Fe from steel ball was low upto 6 N load, but at 8 N load a significant transfer of Fe took place, as shown in Fig. 10. For steel ball, although the amount of Si is negligible, the amount of Ti is quite high (around 20 wt%) and does not show much variation with load.

Summarizing the tribological data and SEM-EDS analysis of worn surfaces, it is evident that a distinct transition in the friction and wear of Ti_3SiC_2 takes place between 6 and 8 N load. Also, the plastic deformation induced damage is more severe at 8 N load compared to abrasion and tribochemical reactions dominated wear process at 6 N load. Because of this important observation, further detailed investigation to characterize the chemistry of tribolayer and the roughness of the worn surface after fretting at 6 and 8 N load were carried out using Raman specterscopy and Atomic force microscopy (AFM).

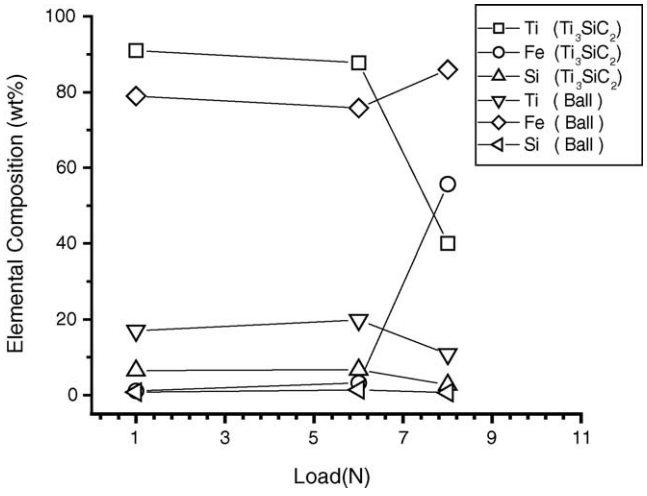

Fig. 10. EDS compositional analysis of fretted surface on Ti_3SiC_2 and steel ball for varying load.

3.2.3. Raman spectroscopy analysis

In order to obtain more information on the chemistry of the tribolayer, Raman spectroscopy analysis is performed for Ti_3SiC_2 samples, fretted at 6 and 8 N (Fig. 11). For 6 N load, the analysis of the Raman spectra, when compared with literature reports,[17,18] shows the evidence of the formation of Fe_2O_3, TiO_2 and SiO_2. On the basis of Raman results, it can be said that the steel ball is severely oxidized and the transfer of oxidized metallic debris takes place during fretting. Also, it is believed that TiC in the investigated Ti_3SiC_2 is presumably oxidized to TiO_2 during fretting and Ti_3SiC_2 oxidizes to

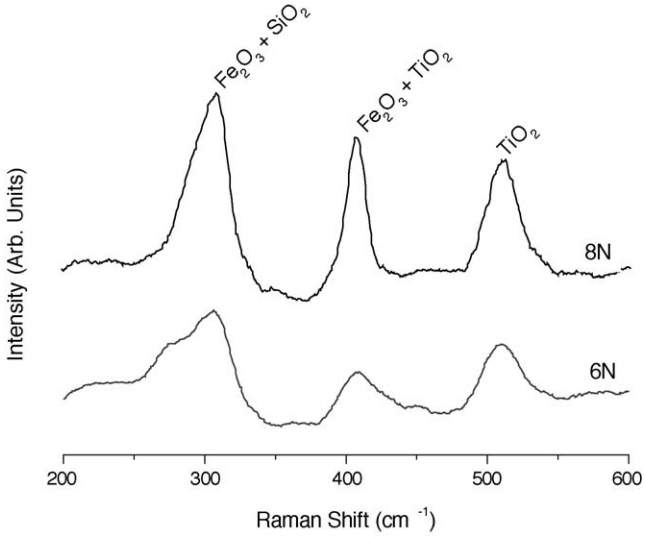

Fig. 11. Raman spectra obtained from the fretted surface on Ti_3SiC_2, worn against steel for 100,000 cycles for different load, as indicated against individual spectrum.

form TiO_2 and SiO_2. Therefore, the tribochemical oxidation taking place during fretting can be understood by following reactions:

$$2Fe + (3/2)O_2 = Fe_2O_3 \quad (1)$$

$$TiC + O_2 = TiO_2 + CO_2(g) \quad (2)$$

$$Ti_3SiC_2 + 6O_2 = 3TiO_2 + SiO_2 + 2CO_2(g) \quad (3)$$

The literature report[22] confirms that the above reaction (3) initiates at 900 °C and the parabolic oxidation behavior in air between 900 and 1400 °C leads to the formation of distinct rutile and silica layers. The activation energy of such reaction under static conditions (e.g. free oxidation in atmosphere) is 370 ± 20 kJ/mol. However, under the dynamic fretting conditions, the driving force for the oxidation reaction (3) will be reduced due to the additional contribution from the frictional energy at the tribocontact.

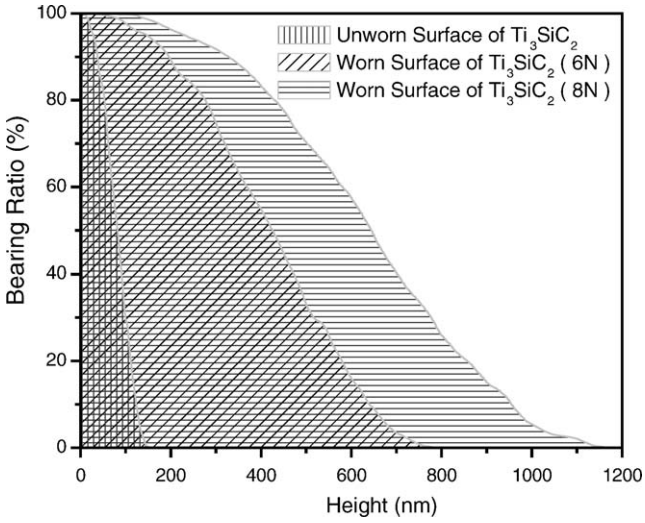

Fig. 12. Bearing area of unworn and worn Ti_3SiC_2 surface, as analyzed by AFM.

3.2.4. AFM analysis

Detailed surface topographical analysis of the worn surfaces is carried out by measuring and characterizing the bearing area curve obtained using AFM. While discussing the AFM results, the concept of bearing area and various important associated parameters will be defined. The bearing area curve is formed by establishing the amount of material a plane would rest on relative to the complete cross section of the surface for each height from the highest to the lowest point of the surface.[25] It gives the material or bearing ratio, which is material-filled length to the evaluation length at the given profile section level. The bearing area curve, measured using AFM is plotted in Fig. 12 and the corresponding roughness parameters are mentioned in Table 2. In Table 2, the various roughness parameters of unworn surfaces are mentioned and the ratios of respective roughness parameter measured on worn surface to that of unworn surface are provided for comparison purpose. Observing roughness data presented in Table 2, it is evident that all the characteristic roughness parameters: S_a, S_q, S_y, S_{pk}, S_k and S_{vk} except S_{sc} when compared with those of unworn surface increase about five times and five to eight times after fretting at 6 and 8 N load, respectively. Also from Table 2, it is clear that the average and root mean square roughness parameters (S_a and S_q) increase with load and that the peak height distribution of the surface asperities are negatively skewed with a considerable fraction of asperities having higher peak height. Since S_{ku} is less than 3, the shape of the peak in amplitude density function (ADF) is flatter compared to a normal Gaussian height distribution. The average peak-to-peak distance (S_y) also increases with normal load, indicating that severity of wear increases and this leads to deformation or removal of more asperities on the tribosurface. Additionally, mean summit curvature (S_{sc}) for surface asperities is observed to decrease with load. As far as other bearing area curve parameters are concerned, the core roughness data (S_k), an alternative measure of surface roughness used for S_a and S_{ku}, is observed to increase by five and six times as load increases from 1 to 6 and 8 N, respectively. The reduced peak height (S_{pk}), corresponding to top 25% material ratio of the worn surface increases to five and eight times with similar variation in fretting load. Larger peak roughness implies that the wear has been more at 8 N load and also the contact stress will be more at 8 N load, which would cause enhanced material removal on further fretting at the interface. The reduced valley height (S_{vk}) corresponding to bottom 25% material ratio also increases with load under the present fretting conditions indicates a larger valley

Table 2
The roughness parameters, as measured using an AFM of unworn and worn surfaces after fretting at 6 and 8 N

Specimen	Unworn surface	Ratio of values measured (worn surface at 6 N: unworn surface)	Ratio of values measured (worn surface at 8 N: unworn surface)
Roughness average, S_a	28 nm	4.96	6.86
Root mean square, S_q	32 nm	5.19	7.31
Surface skewness, S_{sk}	−0.0169	5.30	5.60
Surface kurtosis, S_{ku}	0.446	5.00	5.34
Peak–peak, S_y	153 nm	5.10	7.59
Mean summit curvature, S_{sc}	18.94×10^5 nm	0.20	0.05
Reduced peak height, S_{pk}	16.74 nm	4.86	8.60
Core roughness depth, S_k	98 nm	5.10	6.54
Reduced valley height, S_{vk}	21 nm	5.14	9.43

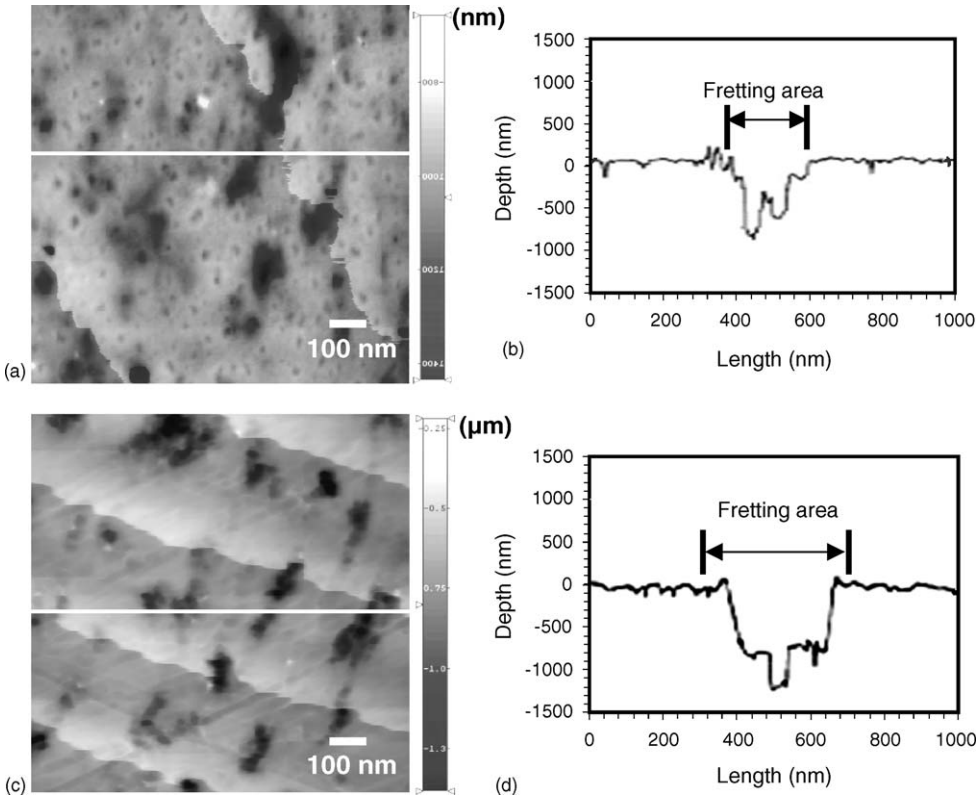

Fig. 13. 2D-AFM image of worn surface topography of Ti_3SiC_2 when fretted against steel ball: (a) 6 N and (c) 8 N. The line profile of Ti_3SiC_2 worn surface: (b) 6 N and (d) 8 N.

depth, leading to the entrapment of more wear debris at the sliding interface. The characteristics of 2D AFM images of the worn surface along with respective line scanned profiles of the selected sections are presented in Fig. 13. From AFM images presented (Fig. 13a and c), it is evident that the worn surface is characterized by severe abrasion, interestingly having grooves of different depths. Also, topographical features indicate that the deformation-induced damage is similar to that of wear of conventional metallic materials, dominated by plastic deformation. Therefore, it is to be understood that the combined effect of severe abrasion along with deformation-induced damage results into the material removal by layers. The depth of the abrasive grooves is found to be around 800 and 1200 nm for the fretting loads of 6 and 8 N, respectively (Fig. 13b and d).

4. Discussion

Based on the tribological data and detailed analysis of topographical features of tribolayer (SEM, Raman and AFM analysis), the mechanism of material removal for Ti_3SiC_2 can be summarized. Three major mechanisms contributing to the process of friction and wear of Ti_3SiC_2 include: (a) abrasion, (b) tribochemical layer formation and (c) plastic deformation.

The experimental results revealed that the steady state COF of Ti_3SiC_2/steel couple increases from 0.55 to 0.6 as load is increased from 1 to 6 N. The increase in COF is presumably due to more severe abrasive action with increased load, as revealed in Fig. 7. However, a decrease in COF from 0.62 to 0.5 is recorded when load is increased from 6 to 8 N and COF remains constant (∼0.5) at 10 N load (Fig. 5). This decrease in COF can be explained as follows. At the higher load (>6 N), the formation of tribochemical reaction products and wear debris takes place to a larger extent. These debris (third body) particles are entrapped in between Ti_3SiC_2 and steel (two first bodies) surfaces and tend to roll during sliding motion, thereby decrease the friction. Hence a transition from two-body to three-body abrasion takes place at load (>6 N), as also observed in Fig. 5.

Another interesting observation is that Ti_3SiC_2, despite having a characteristic chain like unit cell structure, experiences higher COF (0.5–0.6) when compared to other layered structures. The lamellar solids like graphite have hexagonal layer-lattice structure. Their crystal structure is characterized by layers or sheets, within which the bonding between the atoms is covalent and strong. These layers are separated by relatively large distances, and held together by weak Van der Waals type bonding. For MoS_2, the distance between the planes of Mo and S atoms is 1.58 Å and adjacent planes of S atoms are 3.01 Å apart. Typically, the solid lubricants like

graphite, MoS_2 are strongly anisotropic in their mechanical and physical properties. In particular, they are observed to be much less resistant to shear deformation in the basal planes than in other directions. Under the action of a relatively small force, displacement of the layers by easy slippage occurs leading to low COF under ambient humidity (∼40–50%RH) and temperature (23–25 °C). For example, graphite and MoS_2 exhibit low COF of ∼0.2 at RT and COF increases to 0.8 between 400 and 600 °C.[23] It is also reported that h-BN has similarly low COF of 0.2, which is maintained even at higher temperature of 850 °C. The fact that Ti_3SiC_2 has higher COF indicates that similar lubrication mechanism does not operate. This is primarily because of the inherent bond structure, as shown in Fig. 1. It has been reported in literature[24] that the interatomic bond length in Ti (1)–Si is around 2.69 Å, which is lower than the interplanar van der Waals bond length in graphite (3.40 Å). Because of the smaller bond length, the bond strength is expected to be higher in Ti_3SiC_2 than other lamellar solids (MoS_2, graphite), and this explains the difficulty of the slippage of Ti–C–Ti–C–Ti–Si network. It is believed that this contributes to reasonably higher COF (0.5–0.6) of Ti_3SiC_2. It should also be mentioned here that mica, having a characteristic lamellar structure, does not deform easily under shear force and Ti_3SiC_2 also exhibits higher COF than other solid lubricants (WS_2, WSe_2, CdI_2, $(CF_x)_n$, Graphite, MoS_2, PTFE).[25]

As far as the wear behavior is concerned, severe abrasion as well as tribolayer formation is commonly observed for low load regime (1–6 N). The observation of severe abrasion on Ti_3SiC_2, even at lowest load 1 N, is primarily due to the difference in hardness between mating counterfaces. The cracking is not observed on worn Ti_3SiC_2 at 1 N load. At intermediate load of 4 and 6 N, the cracking of the tribolayer is significant and the non-protective nature of the tribolayer increases the wear rate of Ti_3SiC_2. The tribochemical layer at 6 N load is rich in SiO_2 and TiO_2 with little amount of Fe_2O_3. The formation of TiO_2, SiO_2 and Fe_2O_3 is also recorded at 8 N load. A change in wear mechanism is critically observed at high load (8–10 N). It should be noted here that although the tribochemical wear remains an active wear mechanism at load >6 N, the plastic deformation appears to be a significant wear mechanism. At 8 N load, severe plastic deformation contributes to increase in wear rate. Also, the topographical features indicate that the deformation-induced damage is similar to that of wear of conventional metallic materials. The severity of plastic deformation is observed to increase at 10 N load. The deformation of Ti_3SiC_2, as explained in existing literature,[4,5,9,24] can be used to elucidate the observed deformation induced wear of Ti_3SiC_2. In Ti_3SiC_2, two adjacent covalent bond chains of Ti–C–Ti–C–Ti–Si form a chain couple with the length equal to the cell dimension in the *c*-direction (see Fig. 1). The chains are bonded together with strong metallic Ti layers which were found to be inhomogeneous in the free charge density distributions along *c*-axis.[5] Therefore, the deformation behavior of Ti_3SiC_2 at the worn surfaces can also be expected from metallic like bond nature. Also, the interaction between Ti planes is mediated by hexagonal layers of C and Si atoms. Previous investigations report that the Ti (1,2)–C interaction has a stronger covalent p–d nature when compared with the Ti (1)–Si interaction. But, a rigid interaction exists between Si–Si atoms inside Si monolayers.[5,24] Additionally, polar character of the directional bonding reveal the presence of ionic bonding in Ti–C and Ti–Si interactions. This anisotropy of metallic-covalent-ionic bonding was thought to be responsible for the Ti_3SiC_2 plasticity. It is worth to note here that though the Young's modulus (E) of the investigated polycrystalline Ti_3SiC_2 is quite high (316 GPa), the ratio of modulus to hardness (∼63) lies in ductile materials regime.[26] According to Barsoum and co-workers[4,9] plastic deformation of Ti_3SiC_2 was attributed to delamination and kink band formation at above 1200 °C temperature and at room temperature if grains are oriented. Also, our observation that the plastic deformation occurs only at higher load of 8 N indicates that the plasticity of the chain like structure under fretting motion requires a critical contact pressure. The calculated Hertzian contact pressure at 8 N load is around 800 MPa under investigated fretting conditions. Also, the considerable fraction of frictional energy is dissipated as heat energy, which is partitioned at the fretting contact between two mating solids. This evidently increases the contact temperature, depending on the sliding speed as well as thermal properties of two solids in contact. Therefore, it is believed that the combined effect of high contact pressure (at load ≥8 N) and high temperature result in observed plasticity on the worn surfaces of Ti_3SiC_2 under the investigated experimental fretting conditions.

In summary, Ti_3SiC_2 exhibit interesting tribological behavior at varying loads under fretting contacts. A transition in friction and fretting wear rate is critically observed at 6 N load. The observed transition is a result of the interplay among abrasion (two- versus three-body), tribochemical reactions and deformation wear.

5. Conclusions

(a) A transition in COF and wear rate is recorded when load increased from 6 to 8 N. Under the investigated fretting conditions, Ti_3SiC_2/steel tribocouple exhibits high COF (0.5–0.6) and high wear rate (order of 10^{-5} mm^3/N m). At higher load (≥6 N), a decrease in COF is measured along with increase in wear rate.

(b) AFM analysis of the worn surface clearly indicates a considerable increase in roughness parameters (S_a, S_q, S_y, S_{pk}, S_k and S_{vk}) after fretting at 6 N load, when compared to unworn surface. The recorded bearing area curve also correlates well with the increased wear rate at high load (6 and 8 N).

(c) Raman spectroscopy analysis reveals that the fretting wear of investigated tribocouple involves the triboxidation of Ti_3SiC_2 leading to the formation of TiO_2 and

SiO_2. The tribochemical wear, i.e. formation and spalling of layer and severe abrasion of Ti_3SiC_2 are observed as the dominant wear mechanisms at load $\leq$6 N.

(d) At higher load (8 and 10 N), a transition in wear mechanism is noted. Although the tribochemical wear remains active, the plastic deformation induced damage significantly contributes to increased wear rate of Ti_3SiC_2. The deformation at the fretting contact appears to be due to inherent chain structure and metallic bond, characteristic of Ti_3SiC_2.

Acknowledgment

The authors gratefully acknowledge Dr. S.J. Cho, KRISS, Korea for providing the Ti_3SiC_2 test samples.

References

1. Jeitschko, W. and Nowotny, H., Die Kristallstructur von Ti_3SiC_2 – Ein NeuerKomplxcarbid-Typ. *Monatsh. Chem.*, 1967, **98**, 329–337.
2. Barsoum, M. W., The $M_{N+1}AX_N$ phases: a new class of solids thermodynamically stable nanolaminates. *Solid State Chem.*, 2000, **28**(1), 201–281.
3. Murugaiah, A., Souchet, A., El-Raghy, T., Radovic, M., Sundberg, M. and Barsoum, M. W., Tape casting, pressureless sintering, and grain growth in Ti_3SiC_2 compacts. *J. Am. Ceram. Soc.*, 2004, **87**(4), 550.
4. Barsoum, M. W. and Raghy, T. E., Room temperature ductile carbides. *Met. Mat. Trans.*, 1999, **30A**, 363–369.
5. Zhou, Y. and Sun, Z., Electronic structure and bonding properties in layered ternary carbide Ti_3SiC_2. *J. Phys.: Condens. Matter.*, 2000, **12**(28), L457–L462.
6. Barsoum, M. W. and Raghy, T. E., Synthesis and characterization of a remarkable ceramic: Ti_3SiC_2. *J. Am. Ceram. Soc.*, 1996, **79**(7), 1953–1956.
7. Barsoum, M. W., Raghy, T. E., Rawn, C., Porter, W., Wang, H., Payzant, A. *et al.*, Thermal properties of Ti_3SiC_2. *J. Phys. Chem. Solids*, 1999, **60**, 429–439.
8. Raghy, T. E., Zavaliangos, A., Barsoum, M. W. and Kalidindi, S., Damage mechanisms around hardness indentations in Ti_3SiC_2. *J. Am. Ceram. Soc.*, 1997, **80**, 513.
9. Raghy, T. E., Barsoum, M. W., Zavaliangos, A. and Kalidindi, S., Processing and mechanical properties of Ti_3SiC_2. Part II: Mechanical properties. *J. Am. Ceram. Soc.*, 1999, **82**, 2855–2859.
10. Myhra, S., Summers JWB and Kisi, E. H., Ti_3SiC_2 – a layered ceramic exhibiting ultra-low friction. *Mater. Lett.*, 1999, **39**, 6–11.
11. Raghy, T. E., Blau, P. and Barsoum, M. W., Effect of grain size on friction and wear behavior of Ti_3SiC_2. *Wear*, 2000, **238**, 125–130.
12. Zhang Yi, Ding, G. P., Zhou, Y. C. and Cai, B. C., Ti_3SiC_2 – a self-lubricating ceramic. *Mater. Lett.*, 2002, **55**, 285–289.
13. Tang, H. B., Fang, Y. L. and Wang, H. M., Microstructure and dry sliding wear resistance of a $Cr_{13}Ni_5Si_2$ ternary metal silicide alloy. *Acta Mater.*, 2004, **52**(7), 1773.
14. Waterhouse, R. B., Fretting wear. *ASM Handbook*, *Vol. 18*. ASM International, 1992, p. 242.
15. Brown, S. R., ASTM special Technical Publication 780. Warminster, PA, 1982, p. 1.
16. Sarkar, D., Ahn, S., Kang, S. and Basu, B., Fretting wear of TiCN–Ni cermet – influence of secondary carbide content. *P/M Sci. Technol. Briefs*, 2003, **5**(3), 5–11.
17. Serincan, U., Kartopu, G., Guennes, A., Finstad, T. G., Turan, R., Ekinci, Y. *et al.*, Characterization of Ge nanocrystals embedded in SiO_2 by Raman spectroscopy. *Semicond. Sci. Technol.*, 2004, **19**, 247–251.
18. Tjong, S. C., *Mater. Character.*, 1991, **26**, 29.
19. Chen, M., Kato, K. and Adachi, K., Friction and wear of selfmated SiC and Si_3N_4 sliding in water. *Wear*, 2001, **250**, 246–255.
20. Jeng, M. C. and Yan, L. Y., Environmental effects on wear behavior of Al_2O_3. *Wear*, 1993, **161**, 11–16.
21. Hsu, S. M. and Shen, M. C., Ceram. Wear Maps. *Wear*, 1996, **200**, 154–175.
22. Barsoum, M. W., Raghy, T. E. and Ogbuji, L., Oxidation of Ti_3SiC_2 in air. *J. Electrochem. Soc.*, 1997, **144**, 2508–2516.
23. Deacon, R., Lubrication by lamellar solids. *Proc. Roy. Soc.*, 1957, **243A**, 464.
24. Medvedeva, N. I., Novikov, D. L., Ivanovsky, A. L., Kuznetsov, M. V. and Freeman, A. J., Electronic properties of Ti_3SiC_2-based solid solutions. *Phys. Rev. B*, 1998, **58**, 16042–16050.
25. Bhushan, B., *Principles and Applications of Tribology*. John Wiley & Sons, 1999, p. 413.
26. Pampuch, R., Lis, J., Stobierski, L. and Tymkiewicz, M., Solid combustion synthesis of Ti_3SiC_2. *J. Eur. Ceram. Soc.*, 1989, **5**, 283.